Excited states of an electron-hole pair in spherical quantum dots and their optical properties

Takayuki Uozumi and Yosuke Kayanuma
Department of Mathematical Sciences, Graduate School of Engineering, Osaka Prefecture University, Sakai, Osaka 599-8531, Japan
(Received 6 December 2001; revised manuscript received 22 January 2002; published 5 April 2002)

The energy-level structure of a correlated electron-hole pair confined in spherical quantum dots and their optical properties are theoretically investigated. An efficient method of numerical calculation is presented for the eigenvalue problem of the excited states of the electron-hole pair with an arbitrary total angular momentum, which employs the Hylleraas coordinate system and a correlated-basis-set expansion. It is shown that the picture of exciton confinement holds generally when the dot radius is several times larger than the effective Bohr radius of the exciton, but the amount of blue shift in the excited states of the relative motion is larger than that in the lowest *S*-like state. In addition to the one-photon absorption spectra, the excited-state absorption and the two-photon absorption spectra are investigated. The calculated spectra show good agreements with those observed in CuCl nanocrystals.

DOI: 10.1103/PhysRevB.65.165318 PACS number(s): 78.67.Hc

I. INTRODUCTION

Optical properties of semiconductor nanocrystals, or quantum dots (QD's), have been a subject of much interest in recent years.[1] The three-dimensional confinement of electrons and holes drastically changes the electronic structure in QD's from that of bulk crystals with a continuous energy spectrum to that with essentially discretized energy levels. This is called a quantum size effect. Recent advances in material growth and optical measurement techniques allow for the observation of optical responses of an assembly of QD's with a narrow size distribution[2] and even a single QD.[3] The concentration of oscillator strength in discrete energy levels of QD's is a major key in this field, which makes QD's a promising candidate for electro-optic and nonlinear optical applications in the future device technology.

The interacting electrons and holes confined in QD's pose a typical few-body problem and have attracted much theoretical interest. A number of theoretical studies on the electronic structure of QD's have been carried out since the pioneering work by Efros and Efros[4] and Brus.[5] Among these studies, a model of a spherical QD with an effective-mass approximation has been widely used to clarify essential features of quantum size effects.[4,6–12] As a few-body problem, the electron-hole system with an attractive interaction is of interest even in the two-body case because of the presence of bound states. The competition between the attractive Coulomb force and the repulsive confinement force gives rise to a distinct size-dependent change of motional state of the electron-hole pair. This is in contrast to the electron system with repulsive interaction alone, where the main concern is the occurrence of shell structures and the emergence of collective movements. The electronic states of confined two-electron system show only a rather monotonous size dependence.[13,14]

The quantum size effects of an electron-hole pair confined in a spherical QD are characterized by two parameters, the dot radius R and the effective Bohr radius a_B^* of the exciton. There are two extreme situations: the weak, or exciton confinement regime for $R/a_B^* \geqslant 4$ and the strong, or individual particle confinement regime for $R/a_B^* \leqslant 2$.[7] In the former case, the electron-hole pair behaves as an exciton, and its center-of-mass motion is quantized due to the confinement. In the latter case, the kinetic motions of the electron and hole are individually quantized, and a well-separated discretized structure of energy levels are formed, which is slightly modified by the order of $1/R$ due to the Coulomb interaction between electron and hole.

CuCl nanocrystals are typical examples of QD's in the weak confinement regime. The optical properties of this system have been extensively studied from various points of view.[15–18] However, most of these studies are concerned with transitions between the ground state of the nanocrystal and the excited states, although some data on infrared absorption under band-to-band excitation[19] and two-photon excitation spectra[20,21] have also been reported. Recently, Yamanaka *et al.*[22] observed transient infrared absorptions of CuCl QD's embedded in NaCl crystals under size-selective direct excitations. The observed spectra show a characteristic dependence on the dot size, namely, a gradual blue shift of the absorption peak and a remarkable broadening of the spectrum for the smallest size of QD. In a previous paper, we have shown a brief report of the theoretical analysis of these experimental data based on the model of spherical QD with the effective-mass approximation.[23]

The transient absorption spectrum is of special interest, because it contains detailed information on the excited states that cannot be obtained from the direct absorption spectra from the ground state. The interacting electron-hole pair in semiconductors is described by the product of wave functions of the Bloch part and the envelope function. Then, within the long-wavelength limit, the envelope function of the electron-hole pair created optically should have the *S*-like symmetry in spherical QD's with a direct allowed energy gap. The transient absorption at low temperatures, on the other hand, occurs from the lowest *S*-like state. Since the transition dipole moment acts primarily on the envelope function in such an intraband excitation, the final states of transitions in the transient absorption should have *P*-like symmetry. Thus, the information of the *P*-like states can be obtained from the analysis of the transient absorption spec-

tra. An analogous argument holds also for the two-photon absorption process.

Most theoretical studies performed to this time have been concerned with the *S*-like excited states of QD's, while only a few low-lying *P*- and *D*-like excited states have been calculated.[24] In the present paper, we show first a general theoretical framework to calculate the electronic states of an electron-hole pair confined in a spherical QD for excited states with essentially arbitrary total angular momentum L. This scheme proves efficient in calculating electronic states of QD's over a wide range of the dot radius. The obtained accurate eigenstates and eigenvalues form a good basis to calculate the responses of the confined electron-hole pair to various external perturbations. As applications of the scheme, we investigate in detail the one-photon absorption spectra, the transient absorption spectra, and the two-photon absorption spectra in the present paper.

The rest of this paper is organized as follows. In Sec. II, we provide a calculation scheme of the eigenvalue problem for an electron-hole pair confined in spherical QD's with an arbitrary total angular momentum. The formulas for the optical processes are also given here. The results of numerical calculations are given in Sec. III, where the eigenvalues of the electron-hole pair are shown for $L=0,1$, and 2. The dot-size dependence of the optical spectra, the one-photon absorption spectra, the transient absorption spectra, and two-photon absorption spectra, are also shown and discussed here. Finally, the conclusion is given in Sec. IV.

II. FORMULATION

A. Solution of eigenvalue problem

Consider an electron-hole pair confined in a spherical quantum dot with the radius R. The effective-mass Hamiltonian is given by

$$H=\frac{\mathbf{p}_e^2}{2m_e}+\frac{\mathbf{p}_h^2}{2m_h}-\frac{e^2}{\kappa|\mathbf{r}_e-\mathbf{r}_h|}+V(r_e)+V(r_h), \quad (2.1)$$

where $\mathbf{r}_i$, $\mathbf{p}_i$, and m_i are the position, the momentum, and the effective mass of the electron $(i=e)$ and hole $(i=h)$; κ is the dielectric constant of the quantum dot. In this study, we consider a situation of the complete confinement of the particles. Then the confinement potential in Eq. (2.1) is taken as $V(r_i)=0$ for $r_i \leqslant R$ and $V(r_i)=+\infty$ for $r_i>R$, which means that the wave function, the envelope function for the electron-hole pair, vanishes when r_e or r_h is equal to R. It should be noted that our formulation given here can be easily extended to a more general case of confinement potential with spherical symmetry, as mentioned at the end of Sec. II A.

The eigenvalue problem for the Hamiltonian (2.1) is simplified owing to the spherical symmetry of the system. Since both the square $\hbar^2\mathbf{L}^2$ and z component $\hbar L_z$ of the total angular momentum $\hbar\mathbf{L}$ commute with the Hamiltonian, the eigenstates of the system can be classified in terms of a set of quantum numbers (L,M), where $L(L+1)$ and M are the eigenvalues for $\mathbf{L}^2$ and L_z, respectively. Moreover, we can further simplify the eigenvalue problem by describing the system in terms of a coordinate set including the Euler angles. Such a situation is similar to that in the eigenvalue problem for a He atom.[25] A general argument on the symmetry of the eigenstates of the two-electron system of a He atom has been given by Bhatia and Temkin.[26] In the present study, however, we formulate the eigenvalue problem in a different fashion. Our formulation given below is more transparent and best suited to numerical calculations for electron-hole pair systems with a spherical symmetry.

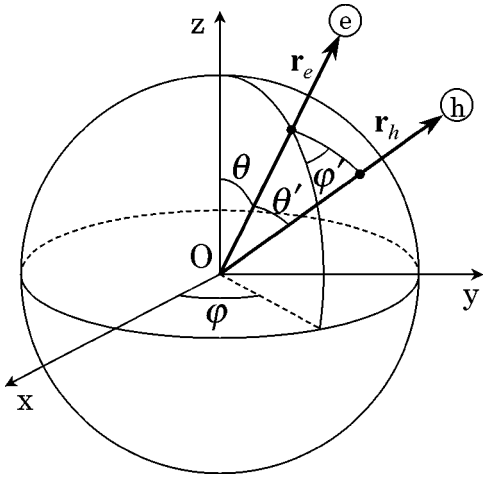

FIG. 1. Coordinate system used in the formalism for an electron-hole pair in a spherical quantum dot.

Figure 1 illustrates the coordinate system employed here. The coordinates are classified into *internal coordinates* and *external coordinates*. The internal coordinates are r_e, r_h, and θ', where θ' is the angle between $\mathbf{r}_e$ and $\mathbf{r}_h$. We may use $r_{eh}=\sqrt{r_e^2+r_h^2-2r_e r_h\cos\theta'}$, the distance between the particles, in place of θ'. The external coordinates are, on the other hand, the Euler angles θ, φ, and φ', where θ and φ are the polar and azimuthal angles for $\mathbf{r}_e$, respectively, and φ' is the angle between the plane including z axis and $\mathbf{r}_e$ and the plane including $\mathbf{r}_e$ and $\mathbf{r}_h$. The eigenvalue problem for Eq. (2.1) is fully simplified by describing the Hamiltonian in the present coordinate system, because the terms concerning with the external coordinates are replaced by several constants related with the angular momentum of the system. The six-dimensional eigenvalue problem for Eq. (2.1) is then essentially reduced to three dimensional one related only with the internal coordinates.

Before going to the formulation, we need to construct simultaneous eigenstates for the angular momentum operators $\mathbf{L}^2$, L_z, and $L_{z'}$, where $L_{z'}$ is the projection of $\mathbf{L}$ in the direction of $\mathbf{r}_e$. These operators are represented in terms of the Euler angles as

$$\mathbf{L}^2=-\frac{1}{\sin^2\theta}\left[\left(\sin\theta\frac{\partial}{\partial\theta}\right)^2+\frac{\partial^2}{\partial\varphi^2}+\frac{\partial^2}{\partial\varphi'^2}-2\cos\theta\frac{\partial^2}{\partial\varphi\partial\varphi'}\right], \quad (2.2)$$

$$L_z=-i\frac{\partial}{\partial\varphi}, \quad (2.3)$$

$$L_{z'}=-i\frac{\partial}{\partial\varphi'}. \tag{2.4}$$

In analogy with a problem for a symmetric top, the simultaneous eigenstate $|L,M,K\rangle$ for these operators is easily constructed, where the integer K is the eigenvalue of $L_{z'}$ and satisfies the condition $|K|\leqslant L$. Actually, $|L,M,K\rangle$ is just the eigenstates of the symmetric top and is described in terms of a hypergeometric function.[27] We need, however, only a formal expression of $|L,M,K\rangle$ as shown below.

We start from $|L,0,K\rangle$. The derivatives of φ in Eq. (2.2) can be omitted in this case, because the eigenfunction of L_z for $M=0$ is a constant $1/\sqrt{2\pi}$. Then Eqs. (2.2) and (2.4) give an expression $Y_{LK}(\theta,\varphi')/\sqrt{2\pi}$ for $|L,0,K\rangle$, where $Y_{LK}(\theta,\varphi')$ is the spherical harmonic function. The other states with $M\neq 0$ are obtained by successive operations of ladder operators $L_\pm$ on $|L,0,K\rangle$, where $L_\pm$ is given by

$$\begin{aligned}L_\pm&=L_x\pm iL_y,\\&=-ie^{\pm i\varphi}\left(\pm i\frac{\partial}{\partial\theta}-\cot\theta\frac{\partial}{\partial\varphi}+\frac{1}{\sin\theta}\frac{\partial}{\partial\varphi'}\right).\end{aligned} \tag{2.5}$$

The operators $L_\pm$ change M into $M\pm 1$, and thus $|L,M,K\rangle$ is given by

$$|L,\pm|M|,K\rangle=\sqrt{\frac{(L-|M|)!}{(L+|M|)!}}L_\pm^{|M|}|L,0,K\rangle. \tag{2.6}$$

Note that $L_\pm$ change only the quantum number M, because $[L_\pm,\mathbf{L}^2]=0$ and $[L_\pm,L_{z'}]=0$.

It is convenient to introduce ladder operators $L_{\pm'}$ for the quantum number K, which are defined as

$$L_{\pm'}=-ie^{\pm i\varphi'}\left(\pm i\frac{\partial}{\partial\theta}-\cot\theta\frac{\partial}{\partial\varphi'}+\frac{1}{\sin\theta}\frac{\partial}{\partial\varphi}\right). \tag{2.7}$$

The operation rule of $L_{\pm'}$ on $|L,M,K\rangle$ is similar to that of $L_\pm$, i.e.,

$$L_{\pm'}|L,M,K\rangle=\sqrt{L(L+1)-K(K\pm1)}|L,M,K\pm1\rangle. \tag{2.8}$$

This is a consequence of the fact that $[L_\pm,L_{\pm'}]=0$ and that commutation relations among $\mathbf{L}^2$, $L_{z'}$, and $L_{\pm'}$ are similar to those among $\mathbf{L}^2$, L_z, and $L_\pm$, which is obvious from the symmetric property of φ and φ' in Eqs. (2.2)–(2.5) and (2.7).

From now on, we adopt the effective Bohr radius $a_B^*\equiv\kappa\hbar^2/\mu e^2$ as the unit of length and the effective Rydberg energy $E_{Ry}^*\equiv\hbar^2/2\mu a_B^{*2}$ as the unit of energy, where μ $[=m_em_h/(m_e+m_h)]$ is the reduced mass. The Hamiltonian in this units is written as

$$H=-c_e\Delta_e-c_h\Delta_h-\frac{2}{r_{eh}}, \tag{2.9}$$

where the coefficients c_e and c_h are $m_h/(m_e+m_h)$ and $m_e/(m_e+m_h)$, respectively. The transformation of Eq. (2.9) into our coordinate system is carried out using the formula,

$$\Delta_i=\frac{\partial^2}{\partial r_i^2}+\frac{2}{r_i}\frac{\partial}{\partial r_i}-\frac{\mathbf{L}_i^2}{r_i^2}, \tag{2.10}$$

where $\mathbf{L}_i$ is the angular momentum of the electron ($i=e$) or hole ($i=h$). The representation for $\mathbf{L}_h^2$ is given by

$$\mathbf{L}_h^2=-\left(\frac{\partial^2}{\partial\theta'^2}+\cot\theta'\frac{\partial}{\partial\theta'}+\frac{1}{\sin^2\theta'}\frac{\partial}{\partial\varphi'^2}\right), \tag{2.11}$$

while that for $\mathbf{L}_e^2$ is obtained from the relation,

$$\mathbf{L}_e^2=\mathbf{L}^2+\mathbf{L}_h^2-2\mathbf{L}_h\cdot\mathbf{L}. \tag{2.12}$$

However, it is more convenient to represent $\mathbf{L}_e^2$ in terms of the angular momentum operators, $\mathbf{L}^2$, $L_{z'}$, and $L_{\pm'}$. This is carried out using an identity,

$$\mathbf{L}_h\cdot\mathbf{L}=-\frac{L_{+'}-L_{-'}}{2}\frac{\partial}{\partial\theta'}+\cot\theta'\frac{L_{+'}+L_{-'}}{2}L_{z'}+L_{z'}^2. \tag{2.13}$$

Finally, from Eqs. (2.10)–(2.13), we obtain the representation of the Hamiltonian in Eq. (2.9) in terms of the present coordinate system,

$$\begin{aligned}H=H_S&+\frac{1}{\sin^2\theta'}\left(\frac{c_e}{r_e^2}+\frac{c_h}{r_h^2}\right)L_{z'}^2+\frac{c_e}{r_e^2}(\mathbf{L}^2-2L_{z'}^2)\\&+\frac{c_e}{r_e^2}\left[(L_{+'}-L_{-'})\frac{\partial}{\partial\theta'}-\cot\theta'(L_{+'}+L_{-'})L_{z'}\right],\end{aligned} \tag{2.14}$$

where H_S is the reduced Hamiltonian for the S-like subspace ($L=0$) and is given by

$$\begin{aligned}H_S=&-c_e\left[\frac{1}{r_e}\frac{\partial^2}{\partial r_e^2}r_e+\frac{1}{r_e^2\sin^2\theta'}\left(\sin\theta'\frac{\partial}{\partial\theta'}\right)^2\right]\\&-c_h\left[\frac{1}{r_h}\frac{\partial^2}{\partial r_h^2}r_h+\frac{1}{r_h^2\sin^2\theta'}\left(\sin\theta'\frac{\partial}{\partial\theta'}\right)^2\right]-\frac{2}{r_{eh}}.\end{aligned} \tag{2.15}$$

The expression for H_S, which has been derived by one of the authors,[6] includes only the internal coordinates. Also the expression for H in Eq. (2.14) essentially includes only the internal coordinates: All the terms concerning with external coordinates have been replaced by the angular momentum operators. In a specific subspace (L,M) for the electron-hole pair, we can replace the angular momentum operators in Eq. (2.14) by constants. Then the originally six-dimensional eigenvalue problem is reduced to three dimensional one concerning only with the internal coordinates. This is an essential advantage of our formulation, which allows for a systematic calculation of the correlated electron-hole pair with an arbitrary angular momentum.

The commutability of H with $\mathbf{L}^2$ and L_z is obvious from Eq. (2.14), since both $\mathbf{L}^2$ and L_z commute with L_i ($i=z',\pm'$). This fact, of course, means that L and M are constants of motion. However, K is not a constant of motion because

the last term in Eq. (2.14) does not commute with $L_{z'}$. In order to show this clearly, we introduce $|L,M,K\rangle_\lambda$ $(\lambda=\pm)$ defined by

$$|L,M,K\rangle_\pm=\frac{1}{\sqrt{2}}[|L,M,K\rangle\pm(-1)^{L+K}|L,M,-K\rangle], \tag{2.16}$$

for $K=1,2,\ldots,L$, and by

$$|L,M,0\rangle_\lambda=|L,M,0\rangle, \tag{2.17}$$

for $K=0$, where λ in Eq. (2.17) is chosen as $+$ $(-)$ when L is an even (odd) integer. The last term in Eq. (2.14) couples $|L,M,K\rangle_\lambda$ with $|L,M,|K\pm1|\rangle_\lambda$, so that K is not a constant of motion. However, it should be noted that λ is unchanged through this coupling, i.e., λ becomes a constant of motion. This means that the vector space for the electron-hole pair is subdivided by the index λ in addition to the angular momentum (L,M). In fact, λ is just the parity of the system: $Y_{L,K}(\theta,\varphi')$ transforms into $(-1)^{L+K}Y_{L,-K}(\theta,\varphi')$ under the spatial inversion I, which is composed of a combined operation of $\theta\to\pi-\theta$, $\varphi\to\pi+\varphi$, and $\varphi'\to\pi-\varphi'$, so that $I|L,0,K\rangle_\pm=\pm|L,0,K\rangle_\pm$. This is also true for $|L,M,K\rangle_\lambda$ with $M\neq0$ because I commutes with $L_\pm$.

As discussed above, the eigenstates of the system are classified in terms of the angular momentum (L,M) and the parity λ. Thus, we expand the wave function of the electron-hole pair in (L,M,λ) subspace in the form

$$\psi_{LM\lambda}(\mathbf{r}_e,\mathbf{r}_h)=\sum_{K=K_0}^{L}f_K^{L\lambda}(r_e,r_h,r_{eh})|L,M,K\rangle_\lambda, \tag{2.18}$$

where K_0 is taken to be $0(1)$ when $\lambda=+$ and L is an even (odd) integer or when $\lambda=-$ and L is an odd (even) integer. Since the operation of angular momentum operators on $|L,M,K\rangle_\lambda$ is easily taken into account using the algebra shown above, the six-dimensional Schrödinger equation, $H\psi_{LM\lambda}(\mathbf{r}_e,\mathbf{r}_h)=E\psi_{LM\lambda}(\mathbf{r}_e,\mathbf{r}_h)$, is transformed into a set of three-dimensional equations for the *internal function* $f_K^{L\lambda}(r_e,r_h,r_{eh})$. Note that the internal function is independent of M because the Hamiltonian does not include L_z. In fact, using the relations, (i) ${}_\lambda\langle L,M,K|L',M',K'\rangle_{\lambda'}=\delta_{L,L'}\delta_{M,M'}\delta_{K,K'}\delta_{\lambda,\lambda'}$, (ii) $L_{z'}|L,M,K\rangle_\lambda=K|L,M,K\rangle_{-\lambda}$, and (iii) $L_{\pm'}|L,M,K\rangle=\sqrt{L(L+1)-K(K\pm1)}|L,M,K\pm1\rangle$, we obtain a set of simultaneous equations,

$$\sum_{K'=K_0}^{L}H_{K,K'}f_{K'}^{L\lambda}(r_e,r_h,r_{eh})=Ef_K^{L\lambda}(r_e,r_h,r_{eh}) \quad (K=K_0,\ldots,L), \tag{2.19}$$

where E is the eigenenergy of the system. The Hamiltonian in Eq. (2.14) changes the quantum number K at most by ±1. Thus, the block element $H_{K,K'}$ in Eq. (2.19) has a tridiagonal form, i.e., $H_{K,K'}=0$ unless $|K-K'|\leqslant1$. The nonzero elements are given as follows:

$$H_{K,K}=H_S+\frac{K^2}{\sin^2\theta'}\left(\frac{c_e}{r_e^2}+\frac{c_h}{r_h^2}\right)+\frac{c_e[L(L+1)-2K^2]}{r_e^2}, \tag{2.20}$$

$$H_{K+1,K}=\frac{c_e\sqrt{L(L+1)-K(K+1)}}{r_e^2}\left(\frac{\partial}{\partial\theta'}-K\cot\theta'\right) \quad (K\geqslant1), \tag{2.21}$$

$$H_{K,K+1}=\frac{c_e\sqrt{L(L+1)-K(K+1)}}{r_e^2}\times\left(-\frac{\partial}{\partial\theta'}-(K+1)\cot\theta'\right) \quad (K\geqslant1), \tag{2.22}$$

$$H_{1,0}=\frac{c_e\sqrt{2L(L+1)}}{r_e^2}\frac{\partial}{\partial\theta'}, \tag{2.23}$$

$$H_{0,1}=\frac{c_e\sqrt{2L(L+1)}}{r_e^2}\left(-\frac{\partial}{\partial\theta'}-\cot\theta'\right). \tag{2.24}$$

Note that each element satisfies a Hermitian relation, $\langle H_{K,K'}\rangle=\langle H_{K',K}\rangle$, which is easily verified by the partial integration with respect to θ'.

From now on, we adopt a conventional notation $S,P,D,\ldots$ for $L=0,1,2,\ldots$. Consider the case for $(L,M,\lambda)=(P,0,-)$, as an example. In this case, the wave function of the electron-hole pair is described by

$$\psi_{P,0,-}(\mathbf{r}_e,\mathbf{r}_h)=\sqrt{\frac{3}{8\pi^2}}[f_0^{P-}(r_e,r_h,r_{eh})\cos\theta-f_1^{P-}(r_e,r_h,r_{eh})\sin\theta\cos\varphi'], \tag{2.25}$$

and we obtain a set of simultaneous equations

$$\sum_{K'=0}^{1}H_{K,K'}f_{K'}^{P-}(r_e,r_h,r_{eh})=Ef_K^{P-}(r_e,r_h,r_{eh}) \quad (K=0,1), \tag{2.26}$$

where

$$H_{0,0}=H_S+\frac{2c_e}{r_e^2},$$

$$H_{1,1}=H_S+\frac{1}{\sin^2\theta'}\left(\frac{c_e}{r_e^2}+\frac{c_h}{r_h^2}\right),$$

$$H_{0,1}=-\frac{2c_e}{r_e^2}\left(\cot\theta'+\frac{\partial}{\partial\theta'}\right),$$

$$H_{1,0}=\frac{2c_e}{r_e^2}\frac{\partial}{\partial\theta'}. \tag{2.27}$$

This is essentially the same as that given in a previous paper.[23]

The eigenvalue problem in Eq. (2.19) is transformed into a diagonalization of the Hamiltonian matrix by expanding the wave function in terms of a set of basis functions. In this study, we employ a *nonorthogonal* correlated basis set,[7]

$$\chi_{lmn}(r_e,r_h,r_{eh})=\varphi_m(r_e/R^*)\varphi_n(r_h/R^*)r_{eh}^l\exp(-\alpha r_{eh}),$$
$$(l=0,1,2,\cdots,\ \text{and}\ \ m,n=1,2,3,\cdots), \tag{2.28}$$

where $R^*\equiv R/a_B^*$, $\varphi_m(x)$ is a $(2m-1)$th order polynomial defined by the Legendre polynomial $P_n(x)$ as $\varphi_m(x)=(1-x)P_{2m-1}(x)/x$, and α is an adjustable parameter chosen to minimize the lowest energy in each (L,M,λ) subspace. By expanding the internal function $f_K^{L\lambda}(r_e,r_h,r_{eh})$ as

$$f_K^{L\lambda}(r_e,r_h,r_{eh})=\sum_{l=0}^{l_{max}}\sum_{m=1}^{m_{max}}\sum_{n=1}^{n_{max}}c_{lmn}^{L\lambda,K}\chi_{lmn}(r_e,r_h,r_{eh}), \tag{2.29}$$

Eq. (2.19) is transformed into an eigenvalue equation for a Hamiltonian matrix represented by nonorthogonal bases, which can be numerically solved by a standard recipe. Note that the boundary condition, $\psi_{LM\lambda}(\mathbf{r}_e,\mathbf{r}_h)=0$ at $r_e=R^*$ or $r_h=R^*$, is automatically satisfied by the choice of $\varphi_m(x)$.

An advantage of the correlated basis expansion is a rapid convergence of low-lying energy levels, owing to the exponential part in Eq. (2.28). This is crucially important for the description of the electron-hole pair, in order to describe the correct behavior of an exciton in the weak confinement regime ($R\gg a_B^*$). The actual calculation has been carried out with a choice, $(l_{max},m_{max},n_{max})=(6,6,6)$, which is enough to obtain converged results at least for relatively low-lying energy levels shown below. The basis function in Eq. (2.28) includes an adjustable parameter α, but the calculated low-lying energy levels are rather insensitive to a moderate change of α. These facts mean that our basis set is almost complete for low-lying eigenstates and guarantees the numerical accuracy beyond simple variational calculations.

Here, we illustrate our formalism to solve the eigenvalue problem for a correlated electron-hole pair confined in a spherical quantum dot for the case with the infinite potential barrier. However, the formulation given above is obviously applicable to the problem with an arbitrary confinement potential barrier with spherical symmetry, for example, the problem with a finite potential barrier.[28] In such a case, we need a proper correlated basis set for the given problem. This is obtained by solving numerically or analytically the problem of one-particle confinement first. Then a nonorthogonal correlated basis set is constructed as the product function among the one-particle wave function for the electron and hole and the binding part of the particles as in Eq. (2.28). The boundary condition for the wave function of the electron-hole pair is obviously satisfied from the beginning by such a choice of the correlated basis set.

B. Optical response of QD's

The optical response of QD's is obtained from the eigenstates and eigenenergies of an electron-hole pair. The one-photon absorption spectrum is calculated, apart from irrelevant factors, by

$$I_1(\omega)=\sum_k |F_k|^2\delta(\omega+E_i-E_{S,+}^{(k)}), \tag{2.30}$$

where E_i and $E_{S,+}^{(k)}$ are the initial and kth S-like state energy, respectively, ω is the photon energy, and $|F_k|^2$ is the oscillator strength per unit volume. Within the effective-mass approximation, the transition amplitude F_k is given by[29]

$$F_k=\sqrt{\frac{\pi a_B^{*3}f_{ex}}{\Omega}}\int d\mathbf{r}\psi_{S,0,+}^{(k)}(\mathbf{r},\mathbf{r}), \tag{2.31}$$

where f_{ex} is the oscillator strength per unit volume for bulk crystals, Ω is the volume of QD, and $\psi_{S,0,+}^{(k)}$ is the wave function of kth S-like state.

The transient absorption process is a kind of two-photon process composed of two successive transitions, the interband transition and the intraband transition. First a valence electron is excited into the conduction band, and the created electron-hole pair relaxes to the lowest S-like state at low temperature. The infrared photons then give rise to the intraband transition of the electron and hole. The infrared absorption spectrum is described by

$$I_{IR}(\omega)=\sum_j |\langle\psi_{P,0,-}^{(j)}|V|\psi_{S,0,+}^{(1)}\rangle|^2\delta(\omega+E_{S,+}^{(1)}-E_{P,-}^{(j)}), \tag{2.32}$$

where $\psi_{P,0,-}^{(j)}$ and $E_{P,-}^{(j)}$ are the jth P^- state and its energy. In this equation, we have assumed, without loss of generality, that the infrared photon is z polarized, i.e., $V=-eE(z_e-z_h)$, where E is the electric field.

The two-photon absorption spectrum is given by

$$I_2(\omega)=\sum_j\left|\sum_k\frac{\langle\psi_{P,0,-}^{(j)}|V|\psi_{S,0,+}^{(k)}\rangle F_k}{\omega+E_i-E_{S,+}^{(k)}+i\gamma}\right|^2\delta(2\omega+E_i-E_{P,-}^{(j)}). \tag{2.33}$$

In this process, the system makes a sequential transition from the initial state to P^- excited states by two photons with the energy ω, which is roughly half of the band-gap energy. In the first excitation, an electron-hole pair with S^+ symmetry is virtually created with the lifetime γ. Then it undergoes a transition to P^- states by the second photon. Here we have assumed that the photons are z polarized. In the present study, we take γ to be 0 and neglect the light-polarization dependence,[30] for simplicity.

The transition amplitudes appeared above can be expressed as integrals for the internal functions $f_K^{L\lambda}$, since the external coordinates are easily integrated using the Wigner-Eckart theorem. The F_k is given by

$$F_k = \sqrt{\frac{2\pi a_B^{*3} f_{ex}}{\Omega}} \int_0^{R^*} r^2 dr f_0^{S+(k)}(r,r,0), \quad (2.34)$$

while $\langle \psi^{(j)}_{P,0,-} | V | \psi^{(k)}_{S,0,+} \rangle$ is given by

$$\langle \psi^{(j)}_{P,0,-} | V | \psi^{(k)}_{S,0,+} \rangle = \frac{a_B^*}{\sqrt{3}} \int_0^{R^*} r_e^2 dr_e \int_0^{R^*} r_h^2 dr_h \times \int_0^{2\pi} \sin\theta' d\theta' f_0^{S+(k)}(r_e, r_h, r_{eh}) \times [(r_e - r_h \cos\theta') f_0^{P-(j)}(r_e, r_h, r_{eh}) - r_h \sin\theta' f_1^{P-(j)}(r_e, r_h, r_{eh})], \quad (2.35)$$

apart from irrelevant factors.

III. NUMERICAL RESULTS

A. Energy scheme of an electron-hole pair

Figures 2(a)–2(c) show the calculated energy levels of an electron-hole pair with S^+, P^-, and D^+ symmetry, respectively, where the effective-mass ratio is taken as $m_h/m_e = 3$. In each figures, only the lowest 24 energy levels are plotted against the radius R of the quantum dot.

The arrows in Figs. 2(a)-2(c) indicate the characteristic levels in the limit of large dot size. These energy levels are rather insensitive to the change of R when R is much larger than a_B^*. In the bulk limit ($R \to +\infty$), these levels approach $-1/n_{ex}^2 E_{Ry}^*$ ($n_{ex} = 1,2$, and 3), the energy of an exciton with the principal quantum number n_{ex}. This behavior clearly illustrates a character of a weakly confined electron-hole pair for $R \gg a_B^*$, which is known as the weak confinement regime, or the exciton confinement regime. In this regime an exciton formed by an electron-hole pair moves in a quantum dot as if it were a single particle. The motional state of an electron-hole pair is then well described as an exciton with quantum numbers $(n_{ex} l_{ex})$ whose center-of-mass motion is quantized due to the confinement with quantum numbers $(n_{CM} l_{CM})$, where l_{ex} and l_{CM} mean the angular momentum of the relative motion and the center-of-mass motion, respectively. We denote the electron-hole pair in the weak confinement regime as $(n_{ex} l_{ex}, n_{CM} l_{CM})_{L\lambda}$. The energy of the pair is approximately given by

$$E_{n_{ex} l_{ex}, n_{CM} l_{CM}} \simeq -\frac{1}{n_{ex}^2} + \frac{\mu \lambda^2_{n_{CM}, l_{CM}}}{M R^{*2}}, \quad (3.1)$$

in the unit of E_{Ry}^*, where $\lambda_{n,l}$ is the nth zero of the lth-order spherical Bessel function and $M(=m_e+m_h)$ is the total mass of the electron and hole. The energy levels approaching $-E_{Ry}^*$ in Fig. 2(b), for example, are assigned as $(1s, n_{CM} P)_{P-}$ state, and those approaching $-1/4\ E_{Ry}^*$ as $(2s, n_{CM} P)_{P-}$, $(2p, n_{CM} S)_{P-}$, or $(2p, n_{CM} D)_{P-}$. It should be noted that such levels as $(2p, n_{CM} P)_{P-}$ do not appear in Fig. 2(b) because the total symmetry P^- cannot be obtained from such a product of states. The energy levels in the other figures are assigned in the similar way: Those of S^+ state are

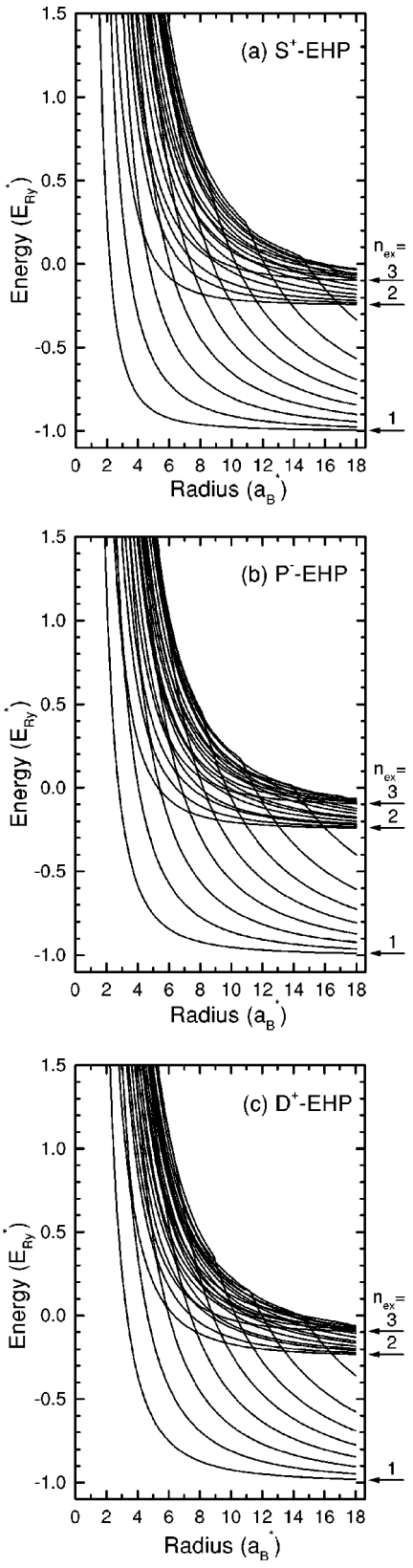

FIG. 2. Energy schemes of a confined electron-hole pair (EHP) with (a) S^+, (b) P^-, and (c) D^+ symmetry. The effective-mass ratio is taken as $m_h/m_e = 3$.

assigned as $(1s,n_{CM}S)_{S+}$, $(2s,n_{CM}S)_{S+}$, $(2p,n_{CM}P)_{S+}$, and so on, while those of D^+ state as $(1s,n_{CM}D)_{D+}$, $(2s,n_{CM}D)_{D+}$, $(2p,n_{CM}P)_{D+}$, $(2p,n_{CM}F)_{D+}$, and so on.

The approximate formula (3.1) for the energy of the electron-hole pair is improved by taking into account the finite size of the exciton. This is known as the dead-layer effect.[7,31] Actually, the center of mass of the exciton cannot reach the surface of the quantum dot because this should accompany a deformation of an exciton that requires so large energy of the order of E_{Ry}^*. Thus the center of mass of the pair is confined in a sphere with the effective radius smaller than R. Equation (3.1) is then improved as

$$E_{n_{ex}l_{ex},n_{CM}l_{CM}} \simeq -\frac{1}{n_{ex}^2} + \frac{\mu\lambda_{n_{CM}l_{CM}}^2}{M(R^*-\eta^*)^2}, \tag{3.2}$$

where $\eta \equiv \eta^* a_B^*$, almost corresponding to the radius of the exciton, is the thickness of the dead layer. In fact, the energy of $(1s,n_{ex}S)_{S+}$ and $(1s,n_{ex}P)_{P-}$ states in the weak confinement regime can be excellently fitted by Eq. (3.2) by choosing $\eta=1.1a_B^*$, and the energy of $(2p,n_{ex}S)_{P-}$ state by choosing $\eta=4.4a_B^*$, for example. Note that these values for η almost correspond to the mean radius for $1s$ exciton ($\langle r\rangle_{1s}=1.5a_B^*$) and that for $2p$ exciton ($\langle r\rangle_{2p}=5a_B^*$).

The concept of an exciton as an elementary excitation loses its meaning when the dot size becomes comparable to or smaller than a_B^* ($R \leqslant a_B^*$), because in this case the kinetic energy of the particles of the order of $1/R^2$ exceeds the Coulomb potential energy of the order of $1/R$. Then the electron-hole pair is well described as a product of one-particle states $(n_i l_i)$ of the electron $(i=e)$ and hole $(i=h)$, which are interacting through the Coulomb force. This is known as the strong confinement regime or the individual confinement regime. The leading terms of the energy of the electron-hole pair in this regime are given by

$$E_{n_e l_e,n_h l_h} \simeq \frac{\mu\lambda_{n_e,l_e}^2}{m_e R^{*2}} + \frac{\mu\lambda_{n_h,l_h}^2}{m_h R^{*2}}, \tag{3.3}$$

in the unit of E_{Ry}^*, where the first and second terms are one-particle energies of the electron and hole. The Coulomb interaction gives rise to the corrections to the above energy of order of R^{-1} and R^0, as discussed in Ref. 7. In the strong confinement regime, the energy levels in Figs. 2(a)–2(c) are denoted as $(n_e s_e, n_h s_h)_{S+}$, $(n_e p_e, n_h p_h)_{S+}$, and so on for S^+ pair, $(n_e s_e, n_h p_h)_{P-}$, $(n_e p_e, n_h s_h)_{P-}$, and so on for P^- pair, and $(n_e s_e, n_h d_h)_{D+}$, $(n_e p_e, n_h p_h)_{D+}$, $(n_e d_e, n_h s_h)_{D+}$, and so on for D^+ pair.

In Figs. 2(a)–2(c), several levels seem to be crossing with each other when R is changed. However, they are not real crossings but avoided crossings, although the energy repulsions are too small, typically $\sim 0.03E_{Ry}^*$, to be resolved in the figures. Such a feature of the avoided level crossings of an electron-hole pair in a quantum dot has been pointed out in Ref. 7, but we reveal here that energy separations at crossings are further smaller than those obtained in the previous study. This improvement is achieved by the use of the larger basis set in the present calculation.

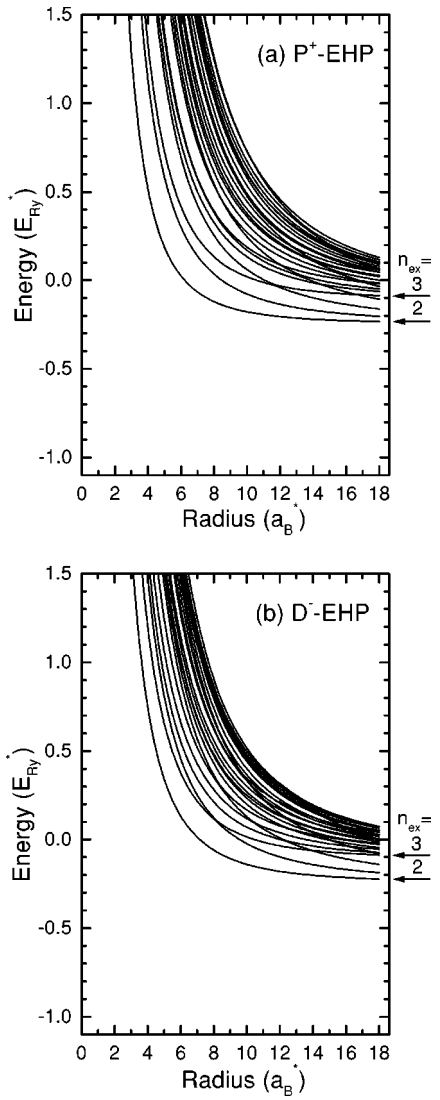

FIG. 3. Energy schemes of a confined electron-hole pair (EHP) with (a) P^+ and (b) D^- symmetry. The effective-mass ratio is taken as $m_h/m_e=3$.

Figures 3(a) and 3(b) show calculated energy levels of an electron-hole pair with symmetry P^+ and D^-, respectively, where the effective-mass ratio is taken as $m_h/m_e=3$. In both figures, only the lowest 24 energy levels are plotted against the quantum dot radius R.

The energy-level structures shown in Figs. 3(a) and 3(b) quite differ from their couterparts with the symmetry P^- and D^+ shown in Figs. 2(b) and 2(c): The energy levels associated with the $1s$ excitonic state are missing in Figs. 3. This remarkable difference between Figs. 2 and 3 is due to the difference in the parity conditions. Consider a P^+ electron-hole pair in the weak confinement regime, for example. In order to make a total angular momentum P, the center-of-mass motion of an $n_{ex}s$ excitons should be $n_{CM}P$. However, such a combination obviously violates the parity condition.

The energy levels in Figs. 3 can be discussed in parallel to Figs. 2 except the difference mentioned above. The electron-hole pair is well described as a product of excitonic state $n_{ex}l_{ex}$ and the center-of-mass motion $n_{CM}l_{CM}$ when R is

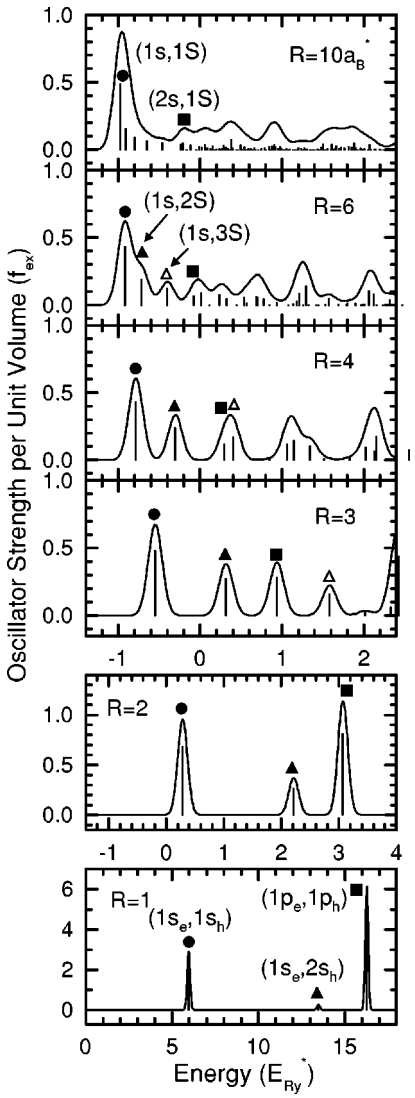

FIG. 4. Dot-size dependence of one-photon absorption spectra of spherical quantum dots. The effective-mass ratio is taken as $m_h/m_e=3$.

larger than several times of a_B^*, i.e., the picture of the exciton confinement holds well also in the present cases. The energy levels in this regime are assigned as $[2p(3p),n_{CM}P]_{P+}$, $(3d,n_{CM}D)_{P+}$, and so on for P^+ pair and as $[2p(3p),n_{CM}D]_{D-}$ and $[3d,n_{CM}P(F)]_{D-}$, and so on for D^- pair. Then the energy of the pair is well described by Eq. (3.2). The picture of the individual confinement also holds in the present cases when the dot radius R is comparable to or smaller than a_B^*, and the levels are assigned as $(n_ep_e,n_hp_h)_{P^+}$, $(n_ed_e,n_hd_h)_{P^+}$, and so on for P^+ pair and as $(n_ep_e,n_hd_h)_{D^-}$, $(n_ed_e,n_hp_h)_{D^-}$, and so on for D^- pair. These *anomalous* parity states are dark states in the sense that they are inactive both in the one-photon and two-photon processes. However they play an important role in the perturbation by an external magnetic field.

B. Optical response of QD's

Figure 4 shows the direct absorption spectra from the groud state of the quantum dots, where the effective-mass ratio is taken as $m_h/m_e=3$ and the dot size R is changed from $1a_B^*$ to $10a_B^*$. In each panels, the vertical lines are the oscillator strength per unit volume calculated from Eq. (2.31), and the continuous lines are the convolution of the vertical lines with a Gaussian function with the half width, $0.1E_{Ry}^*$, at the half maximum (HWHM). The spectra show a drastic change when R is reduced from $10a_B^*$. The overall feature in the spectral change, such as the blue shift of the lines and the enhancement of the oscillator strength due to the confinement of particles, is similar to that obtained in Ref. 7. In bulk crystals of semiconductors with the direct allowed gap, only the excitonic state $n_{ex}s$ with the zero-translational momentum can be excited in the one-photon absorption process because of the momentum conservation. The transition probability is then in proportion to $1/n_{ex}^3$. Such a transition is found in the spectrum for $R=10a_B^*$ as the marked lines, where the line marked by a solid circle corresponds to the transition to $(1s,1S)_{S+}$ state and the line marked by a solid square corresponds to the transition to $(2s,1S)_{S+}$ state. We also see a series of lines corresponding to the transition to $(1s,n_{CM}S)_{S+}(n_{CM}=2,3,\cdots)$ on the high-energy side of the $(1s,1S)_{S+}$ line in the spectrum for $R=10a_B^*$. These transitions are accompanied by the excitation of the center-of-mass motion and become optically allowed because of the breaking of the translational symmetry. From Eq. (2.31), the oscillator strength per unit volume for such transitions in the weak confinement regime is given by

$$\frac{6f_{ex}}{\pi^2 n_{CM}^2}\left(1-\frac{\eta}{R}\right)^3,$$

where the term η/R originates from the dead-layer effect. From the formula $\Sigma_{n=1}1/n^2=\pi^2/6$, we see that the oscillator strength f_{ex} in the bulk limit is distributed over the center-of-mass excitation in QD's. The $1/n_{CM}^2$ dependence was first pointed out by Efros and Efros.[4]

When the dot size is reduced from $R=10a_B^*$, the order of the levels is interchanged at avoided crossings shown in Fig. 2(a), and the transition probability of the low-lying levels become to deviate from the $1/n_{ex}^3$ and $1/n_{CM}^2$ dependence discussed above. By tracing the line corresponding to $(1s,2S)_{S+}$ state (solid triangle) and the line corresponding to $(2s,1S)_{S+}$ state (solid square) from the weak confinement regime to the strong confinement regime passing through the avoided crossings, we find that the former continuously changes into the $(1s_e,2s_h)_{S+}$ state in the strong confinement regime, while the latter changes into the $(1p_e,1p_h)_{S+}$ state. However, these correspondences between the character of the two lines are not unique but depend on the mass ratio m_h/m_e. When $m_h/m_e\leqslant 1.9$, $(1s,2S)_{S+}$ state changes into $(1p_e,1p_h)_{S+}$ state and $(2s,1S)_{S+}$ into $(1s_e,2s_h)$, as discussed in Ref. 7. This is important for the assignment of the lines in the strong confinement regime, because the transition to $(1p_e,1p_h)$ state is optically allowed but the transition to $(1s_e,2s_h)$ state is forbidden, as clearly seen in the lowest

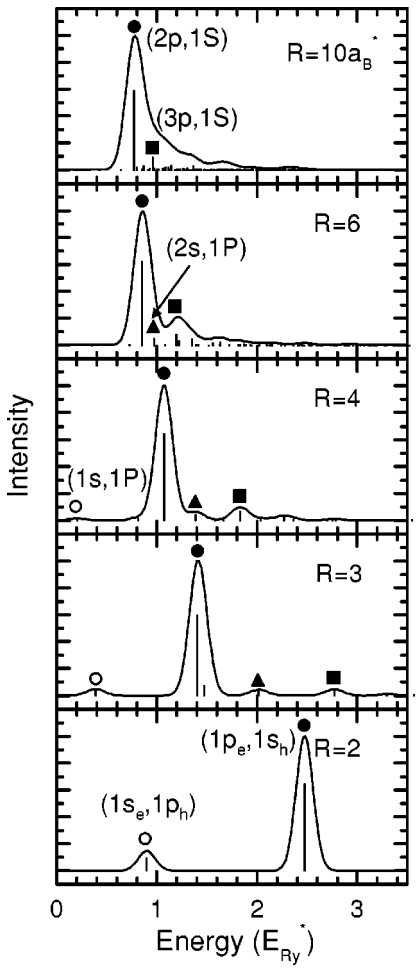

FIG. 5. Dot-size dependence of transient absorption spectra of spherical quandtum dots. The effective-mass ratio is taken as $m_h/m_e=3$.

panel of Fig. 4. See how the absorption spectrum changes to a series of well-isolated discrete lines as the dot size is reduced.

Figure 5 shows the dot-size dependence of the transient absorption spectrum. The effective-mass ratio is taken as $m_h/m_e=3$. The vertical lines in each panels are the normalized oscillator strength obtained from Eq. (2.35). The continuous spectra are obtained by convoluting the vertical lines with the Gaussian function with $0.1E_{Ry}^*$ width (HWHM). In the spectrum for $R=10a_B^*$, the main line marked by a solid circle corresponds to the excitation of the internal motion of the exciton from $1s$ state to $2p$ state, while the line marked by a solid square corresponds to the excitation to $3p$ state. As the dot size is reduced, the main line gradually shifts to the high-energy side. This is attributed to the difference between the quantum size effect for $1s$ state and $2p$ state. In the weak confinement regime, the initial-state energy and the final-state energy corresponding to the main line are given by

$$E_{1s,1S}=-1+\frac{\pi^2\mu}{M(R^*-\eta_{1s}^*)^2}, \tag{3.4}$$

$$E_{2p,1S}=-0.25+\frac{\pi^2\mu}{M(R^*-\eta_{2p}^*)^2}, \tag{3.5}$$

in the unit of E_{Ry}^* from Eq. (3.2). The values of $\eta_{1s}^*a_B^*$ and $\eta_{2p}^*a_B^*$ are estimated as $1.1a_B^*$ and $4.4a_B^*$, respectively, by fitting the energy levels in Figs. 2(a) and 2(b) with above equations, i.e., the effective radius of $2p$ excitonic state is larger than that of $1s$ state. This fact means that the dead-layer effect becomes stronger for $2p$ state than for $1s$ state and thus causes the peak blue shift observed here. We also see a transition to the $(2s,1P)_{P-}$ state marked by a solid triangle, which gains a weak oscillator strength because of the breakdown of the translational symmetry. The size dependence of the transient absorption spectra calculated here reproduces fairly well the data observed for CuCl QD's embedded in NaCl crystals[22,23] without adjustable parameters. The applicability of the complete-confinement model to this system is partly owing to the wide band gap of the host material, i.e., the band-gap energy of about 8.6 eV of NaCl crystals[32] is sufficiently larger than that of about 3.4 eV of CuCl crystals.

As the dot size is further reduced, the blue shift of the main line becomes salient. In the limit of strong confinement, absorption lines are assigned as the individual excitations of the confined electron and hole. For example, the two lines in the bottom panel correspond to the transition of the electron $1s_e\rightarrow 1p_e$ (solid circle) and the hole $1s_h\rightarrow 1p_h$ (open circle) from the initial state $(1s_e,1s_h)_{S+}$. Here, it is instructive to see that the transition dipole $\mathbf{V}$ for the infrared excitation can be written in two ways,

$$\mathbf{V}=-e\mathbf{r}_{eh}=-e\mathbf{r}_e+e\mathbf{r}_h. \tag{3.6}$$

Namely, it is regarded as the polarization with respect to either the center of mass of the exciton, or the center of the dot. Thus we can see the change of the picture of the induced polarization from the former to the latter as the dot size is reduced.

In the strong confinement regime, the intensity ratio between the lines corresponding to $(1s_e,1p_h)_{P-}$ (open circle) and $(1p_e,1s_h)_{P-}$ state (solid circle) strongly depends on the mass ratio m_h/m_e as shown in Fig. 6, where the spectra are calculated for $m_h/m_e=1$,3, and 5 and for $R=a_B^*$. In the case of $m_e=m_h$, the lowest excitation becomes optically forbidden. This is because of the following reason. When $m_e=m_h$, the excited states $(1s_e,1p_h)_{P-}$ and $(1p_e,1s_h)_{P-}$ become degenerate in the zeroth-order approximation. This degeneracy is removed by the Coulomb interaction between the particles. Then, the lowest excited state is symmetric with respect to the exchange of $\mathbf{r}_e$ and $\mathbf{r}_h$ because of the attractive interaction between the particles, while the second excited state has the antisymmetric property. Since the symmetric state has no polarization, the lowest state becomes optically forbidden in the infrared excitation.

Figure 7 summarizes the dot-size dependence of the blue shift of the main line in Fig. 5 (solid circles), where the excitation energy is shown by the solid curve. In this figure, we also show the excitation energy under the exciton confinement picture (dotted curve) and that under the individual

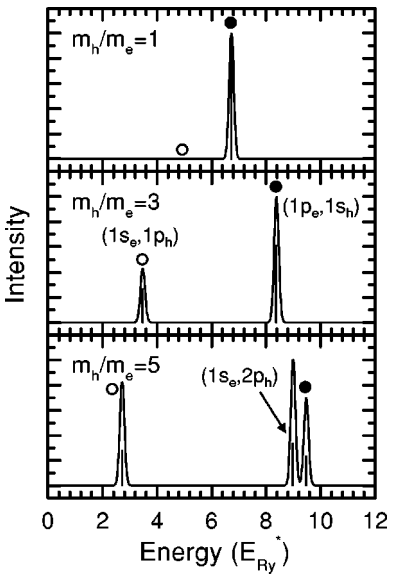

FIG. 6. Transient absorption spectra of spherical quantum dots with the radius $R=a_B^*$. The effective-mass ratio is taken as $m_h/m_e=1$,3, and 5.

particle confinement picture (dashed curve). The former is estimated from Eqs. (3.4) and (3.5), while the latter is estimated from the approximate energies,

$$E_{1s_e,1s_h}=\frac{\pi^2}{R^{*2}}-\frac{3.572}{R^*}, \tag{3.7}$$

$$E_{1p_e,1s_h}=\frac{\mu\pi^2}{m_eR^{*2}}+\frac{\mu\lambda_{1p}^2}{m_hR^{*2}}-\frac{3.240}{R^*}, \tag{3.8}$$

for initial and final state energies in the unit of E_{Ry}^*, where $\lambda_{1p}=4.493$ and the coefficients for the Coulomb potential are numerically estimated. Figure 7 clearly shows how the

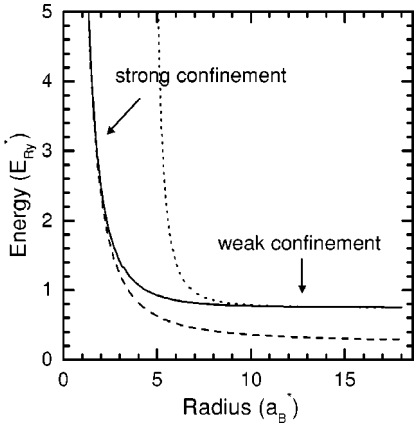

FIG. 7. Dot-size dependence of the excitation energy in the transient absorption spectra (solid line). The excitation energies in the exciton confinement picture (dotted line) and the individual particle confinement picture (dashed line) are also shown.

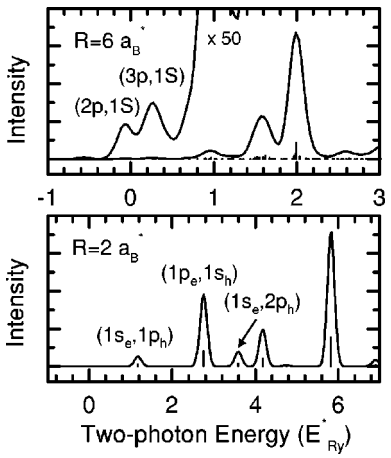

FIG. 8. Two-photon absorption spectra of spherical quantum dots. The dot radius is taken as $R=2a_B^*$ and $6a_B^*$, and the effective-mass ratio is taken as $m_h/m_e=3$.

main line in the transient absorption spectrum shifts from the weak confinement regime to the strong confinement regime when the dot size is reduced.

Figure 8 shows the two-photon absorption spectra calculated for $R=6a_B^*$ and $2a_B^*$. In this calculation we take the effective-mass ratio as $m_h/m_e=3$ and the band energy gap as 3.4 eV, assuming the case of CuCl dots. The spectrum for the weak confinement regime ($R=6a_B^*$) is significantly different from that for the srtong confinement regime ($R=2a_B^*$). In the spectrum for $R=6a_B^*$, we see the low-lying lines corresponding to the transition to $2p$ and $3p$ excitonic state and the wide absorption bands with a strong intensity on the high-energy side. On the other hand, the spectrum for $R=2a_B^*$ is composed of the well isolated lines, where the lowest excited line corresponds to the transition to $(1s_e,1p_h)_{P^-}$ state and the second one corresponds to the transition to $(1p_e,1s_h)_{P^-}$ state. It is interesting to compare the two-photon absorption spectra in Fig. 8 with the transient absorption spectra in Fig. 5. These spectra show quite different structure from each other, though they have common final states of the electron-hole pair with P^- symmetry. The difference between the two-photon absorption and the transient absorption comes from the difference of the intermediate state in both processes. In the transient absorption, the system relaxes to the lowest state of the S^+-like electron-hole pair in the intermediate states. However, the two-photon absorption occurs as a coherent second-order process described in Eq. (3.1), so that essentially all of the S^+-like states contribute to the absorption process as intermediate states. The spectral feature that the intensity steeply uprises in the higher-energy side in the two-photon absorption presented here agrees with that of the observed data for CuCl nanocrystals embedded in NaCl.[33,34]

IV. CONCLUSION

In this work, we presented an efficient formalism to solve numerically an attractive two-body problem confined in spherical nanospaces. The spherical symmetry of the system

was fully exploited in the formalism. The correlated-basis-set expansion of the wave function is successfully applied to the eigenvalue problem of an electron-hole pair confined in spherical quantum dots. It should be noted that, in the case of the attractive interaction, there is no region of ''low density limit'' because of the presence of bound states. Therefore, it is crucially important to take into account the formation of quasiparticle (exciton) from the beginning of the calculation, especially in the weak confinement regime. The features of optical spectra such as the direct one-photon absorption, the transient infrared absorption, and the two-photon absorption observed in CuCl nanocrystals were consistently reproduced by the theoretical calculation given here.

In the present study, we have adopted a simple model of confined electron and hole interacting through the attractive Coulombic force, in order to clarify the essential features of the quantum size effects and the size-dependent optical responses. We would like to stress here that the establishment of the method to calculate essentially *all* of the relatively low-lying eigenstates of the electron-hole pair opens a possibility to calculate responses of the system to various perturbations with a high accuracy. In fact, various perturbative effects may become important for the analysis of actual experimental data. For example, it has been proposed that a two-photon transition to the longitudinal exciton state is induced by the quantum confinement and plays a role in the size-selective two-photon luminescence of CuCl nanocrystals.[21] This poses an interesting problem, i.e., the resonant interaction of electromagnetic fields with a confined electron-hole system. This is also related with a conjecture of the enhancement of the exchange interaction by the quantum confinement.[35] In this connection, Ajiki and Cho[36] recently performed a theoretical study of LT splitting of a confined exciton by approximating the exciton as a point dipole. This approximation is valid in the limit of the weak confinement. We have recently carried out the calculation of the eigenstates of the coupled mode of the confined electron hole with electromagnetic fields, on the basis of the present formalism, where the wave function of the system is systematically expanded to the linear combination of the unperturbed eigenstates. The detail of such a study will be shown elsewhere.

As another example, we may mention the persistent hole burning[18] and the blinking observed in some nanocrystals.[37–39] The origin of these phenomena is attributed to the perturbation by external point charges that are ejected somehow outside the quantum dots.[18] In our preliminary report,[40] we have shown the effects of an external point charge on the wave function of the confined electron-hole system. It has been found that the deformation of the confined electron-hole wave function due to the electric field strongly suppresses the transition probability. A systematic investigation of such an effect will be presented in the forthcoming papers.

ACKNOWLEDGMENTS

We thank Professor T. Itoh and Professor K. Edamatsu for valuable discussions and for sharing the experimental data before publication. This work was partially supported by the Grant in Aid for Scientific Research from the Ministry of Education, Science, Sports, and Culture of Japan.

[1] See, for instance, *Optical properties of Semiconductor Quantum Dots*, edited by U. Waggon (Springer, Berlin, 1997); *Optical Properties of Semiconductor Nanocrystals*, edited by S. V. Gaponenko (Cambridge University Press, Cambridge, 1998).
[2] M.G. Bawendi, W.L. Wilson, L. Rothberg, P.J. Carroll, T.M. Jedju, M.L. Steigerwald, and L.E. Brus, Phys. Rev. Lett. **65**, 1623 (1990).
[3] M. Nirmal, B.O. Dabbousi, M.G. Bawendi, J.J. Macklin, J.K. Trautman, T.D. Harris, and L.E. Brus, Nature (London) **383**, 802 (1996); M. Grundmann, J. Christen, N.N. Ledentsov, J. Böhrer, D. Bimberg, S.S. Ruvimov, P. Werner, U. Richter, U. Gösele, J. Heydenreich, V.M. Ustinov, A.Yu. Egorov, A.E. Zhukov, P.S. Kop'ev, and Zh.I. Alferov, Phys. Rev. Lett. **74**, 4043 (1995).
[4] Al.L. Efros and A.L. Efros, Fiz. Tekh. Poluprovdn. **16**, 1209 (1982) [Sov. Phys. Semicond. **16**, 772 (1982)].
[5] L.E. Brus, J. Chem. Phys. **80**, 4403 (1984).
[6] Y. Kayanuma, Solid State Commun. **59**, 405 (1986).
[7] Y. Kayanuma, Phys. Rev. B **38**, 9797 (1988).
[8] T. Takagahara, Phys. Rev. B **39**, 10 206 (1989).
[9] P.E. Lippens and M. Lannoo, Phys. Rev. B **39**, 10 935 (1989).
[10] Y.Z. Hu, M. Lindberg, and S.W. Koch, Phys. Rev. B **42**, 1713 (1990).
[11] M.V. Rama Krishna and R.A. Friesner, Phys. Rev. Lett. **67**, 629 (1991).
[12] G.T. Einevoll, Phys. Rev. B **45**, 3410 (1992).
[13] M. Taut, Phys. Rev. A **48**, 3561 (1993).
[14] B. Szafran, J. Adamowski, and S. Bednarek, Physica E (Amsterdam) **4**, 1 (1999).
[15] A.I. Ekimov, Al.L. Efros, and A.A. Onushchenko, Solid State Commun. **56**, 921 (1985).
[16] T. Itoh, Y. Iwabuchi, and M. Kataoka, Phys. Status Solidi B **145**, 567 (1988).
[17] K. Edamatsu, J. Lumin. **70**, 377 (1996).
[18] Y. Masumoto, J. Lumin. **70**, 386 (1996).
[19] Y. Miura, K. Edamatsu, and T. Itoh, J. Lumin. **66&67**, 401 (1996).
[20] K. Edamatsu, K. Hisakawa, and T. Itoh, J. Lumin. **72-74**, 329 (1997).
[21] A.V. Baranov, Y. Masumoto, K. Inoue, A.V. Fedorov, and A.A. Onushchenko, Phys. Rev. B **55**, 15 675 (1997).
[22] K. Yamanaka, K. Edamatsu, and T. Itoh, J. Lumin. **76&77**, 256 (1998).
[23] T. Uozumi, Y. Kayanuma, K. Yamanaka, K. Edamatsu, and T. Itoh, Phys. Rev. B **59**, 9826 (1999).
[24] S.V. Nair and T. Takagahara, Phys. Rev. B **53**, R10 516 (1996).
[25] E.A. Hylleraas, Z. Phys. **54**, 347 (1929).
[26] A.K. Bhatia and A. Temkin, Rev. Mod. Phys. **36**, 1050 (1964).
[27] *Method of Theoretical Physics*, edited by M. Morse and H. Feschbach (McGraw-Hill, New York, 1953), p. 1721.
[28] Y. Kayanuma and H. Momiji, Phys. Rev. B **41**, 10 261 (1990).

[29] C.H. Henry and K. Nassau, Phys. Rev. B **1**, 1628 (1970).
[30] A.V. Fedorov, A.V. Baranov, and K. Inoue, Phys. Rev. B **54**, 8627 (1996).
[31] J.J. Hopfield and D.G. Thomas, Phys. Rev. **132**, 563 (1963).
[32] K. Teegarden and G. Baldini, Phys. Rev. **155**, 896 (1967).
[33] K. Edamatsu, K. Hisakawa, and T. Itoh, Phys. Rev. B **59**, 15 868 (1999).
[34] T. Itoh, K. Yamanaka, K. Edamatsu, T. Uozumi, and Y. Kayanuma, in *Proceedings of 2000 International Conference on Excitonic Processes in Condensed Matter*, edited by K. Cho and A. Matsui (World Scientific, Singapore, 2001), p. 1.
[35] A. Fujii, T. Ono, W. Yu, and R. Maki, in *Proceedings of 2000 International Conference on Excitonic Processes in Condensed Matter* (Ref. 34), p. 201.
[36] H. Ajiki and K. Cho, Phys. Rev. B **62**, 7402 (2000).
[37] M. Sugisaki, H.-W. Ren, S.V. Nair, J.-S. Lee, S. Sugou, T. Okuno, and Y. Masumoto, J. Lumin. **87-89**, 40 (2000).
[38] Al.L. Efros and M. Rosen, Phys. Rev. Lett. **78**, 1110 (1997).
[39] K.T. Shimizu, R.G. Neuhauser, C.A. Leatherdale, S.A. Empedocles, W.K. Woo, and M.G. Bawendi, Phys. Rev. B **63**, 205316 (2001).
[40] T.Uozumi and Y. Kayanuma, in *Proceedings of 2000 International Conference on Excitonic Processes in Condensed Matter* (Ref. 34), p. 421.